

# PHOTONICS Research

## Solitons in the fractional Schrödinger equation with parity-time-symmetric lattice potential

XIANKUN YAO AND XUEMING LIU\*

State Key Laboratory of Modern Optical Instrumentation, Department of Optical Engineering, Zhejiang University, Hangzhou 310027, China

\*Corresponding author: liuxm1972@163.com

Received 11 June 2018; revised 5 July 2018; accepted 8 July 2018; posted 11 July 2018 (Doc. ID 334753); published 13 August 2018

We investigate the properties of spatial solitons in the fractional Schrödinger equation (FSE) with parity-time (PT)-symmetric lattice potential supported by the focusing of Kerr nonlinearity. Both one- and two-dimensional solitons can stably propagate in PT-symmetric lattices under noise perturbations. The domains of stability for both one- and two-dimensional solitons strongly depend on the gain/loss strength of the lattice. In the spatial domain, the solitons are rigidly modulated by the lattice potential for the weak diffraction in FSE systems. In the inverse space, due to the periodicity of lattices, the spectra of solitons experience sharp peaks when the values of wavenumbers are even. The transverse power flows induced by the imaginary part of the lattice are also investigated, which can preserve the internal energy balances within the solitons. © 2018 Chinese Laser Press

**OCIS codes:** (190.6135) Spatial solitons; (070.2575) Fractional Fourier transforms; (190.3270) Kerr effect.

<https://doi.org/10.1364/PRJ.6.000875>

### 1. INTRODUCTION

Fractional quantum mechanics, a promising extension of quantum mechanics, is a fascinating subject and has been widely studied [1,2]. Laskin formulated the fractional Schrödinger equation (FSE) to describe the fractional quantum mechanics when the Brownian trajectories in Feynman path integrals are replaced by Lévy trajectories [3,4]. Subsequently, the condensed-matter scheme of space-fractional quantum mechanics was proposed in a one-dimensional Lévy crystal [5]. In 2015, the first optical realization of the FSE was achieved in aspherical optical cavities by Longhi [6], who realized the fractional quantum harmonic oscillator in an aspherical optical cavity, in which dual Airy beams were generated. Subsequently, the propagation dynamics of wave packets were reported in FSEs with parabolic potential [7], Kerr nonlinearity [8], double-barrier potential [9,10], and no potential involved [11]. In recent years, the nonlinear FSE has attracted great attention. Some examples, such as the standing-waves solution [12], quasi-soliton behavior [8], the proof of existence of a soliton solution [13], and bound states [14], were mathematically investigated in various forms of the nonlinear fractional Schrödinger equation (NFSE). In particular, the gap solitons and surface gap solitons in the NFSE were reported in the finite bandgaps of lattices for different Lévy indexes [15,16].

As with fractional quantum mechanics, parity-time (PT) symmetry also initially began as an extension of quantum mechanics. The PT-symmetric Hamiltonians can exhibit a real eigenvalue spectrum in spite of the fact that they are non-Hermitian [17,18]. A necessary condition for a Hamiltonian to be PT

symmetric is the potential function satisfying  $V(x) = V^*(-x)$ . In particular, the spectra of a PT-symmetric system possess a phase transition point above which the spectra become partially or completely complex and the PT symmetry is broken [19]. Beam propagation in PT-symmetric lattices can show a wide variety of interesting effects, such as double refraction, power oscillations, and nonreciprocity [18,20–23]. Particularly, solitons can stably propagate in PT-symmetric lattices that are described by the ordinary nonlinear Schrödinger equation (NSE) along with their associated transverse power flow [24,25].

The combination of the FSE and PT symmetry is an interesting topic. Recently, PT symmetry in the spatial FSE was reported by Zhang *et al.*, who showed that the nondiffracting propagation and conical diffraction of input beams were found at the critical point of a PT-symmetric lattice [26]. More recently, Dong *et al.* have investigated double-hump solitons in the 1D NFSE with PT-symmetric potentials, and they found that the out-of-phase and in-phase solitons can be stable in focusing media and defocusing media, respectively [27]. Up to now, neither the combination of PT symmetry and lattice nor the higher-dimension solitons in the NFSE have been reported. That is what we will address in this paper.

In this work, we investigate the soliton solutions that exist in the NFSE with PT-symmetric lattice potential for a Lévy index of  $\alpha = 1$ . Both 1D and 2D solitons in the semi-infinite forbidden gaps of lattices can stably propagate long distances under noise perturbations in the stable ranges of propagation constants. Combined with the characteristics of PT-symmetric

lattice potentials, we study the spatial domain and inverse space distributions of solitons. The imaginary part of the lattice induces the transverse power flow that flows from gain to loss regions within the solitons. The existence ranges of stable solitons are also investigated by linear stability analysis.

## 2. ONE-DIMENSIONAL SOLITONS

The self-focusing Kerr nonlinear FSE is written as

$$i \frac{\partial \psi}{\partial z} - \left( -\frac{\partial^2}{\partial x^2} \right)^{\alpha/2} \psi + V(x)\psi + |\psi|^2 \psi = 0, \quad (1)$$

where  $\alpha$  is the Lévy index ( $1 < \alpha \leq 2$ ), and  $V(x)$  is the periodic PT-symmetric potential. Physically,  $\text{Re}\{V(x)\}$  is associated with index guiding, while  $\text{Im}\{V(x)\}$  represents the gain or loss distribution of the optical medium. For the sake of universality, we consider the potential function of the form  $V(x) = A[\cos^2(x) + iV_i \sin(2x)]$  with amplitude  $A = 1$  and a parameter  $V_i$  to be varied. Clearly, the period of the potential is  $D = \pi$ . When  $\alpha = 2$ , Eq. (1) recovers the ordinary NSE. In this work, we explore the limiting case of  $\alpha = 1$ .

Before finding the soliton solutions of Eq. (1), we first explore the linear properties of the periodic potential in the FSE. The solution of Eq. (1) without the Kerr nonlinear term can be written in the form  $\psi(z, x) = \phi_k(x) \exp(i\beta z + ikx)$ , where  $\phi_k(x)$  is the Bloch mode, and  $\beta$  is the propagation constant. The photonic band structure can be obtained by the plane-wave expansion method. Since the potential  $V(x)$  is  $\pi$ -periodic, according to the Floquet–Bloch theorem,  $\phi_k$  is spatially periodic for  $\phi_k(x) = \phi_k(x + D)$ . The potential  $V(x)$  and Bloch mode  $\phi_k$  can be expanded into a series of plane waves:  $\phi_k = \sum_m A_m \exp(iK_m x)$  and  $V(x) = \sum_m B_m \exp(iK_m x)$  with  $K_m = 2m\pi/D$ , where  $A_m = \int_0^D \phi_k(x) \exp(-iK_m x) dx / D$  and  $B_m = \int_0^D V(x) \exp(-iK_m x) dx / D$ . Substitution of these series into the linear version of Eq. (1) yields the linear eigenvalue problem

$$\sum_n A_{m-n} B_n - |k + K_m|^\alpha A_m = \beta A_m, \quad (2)$$

which is an eigenvalue problem in matrix form. The band structure for the linear version of Eq. (1) can be obtained for certain  $\alpha$ . For PT-symmetric lattice potentials, the band spectrum can be purely real, as the system is operated below the phase transition point. Here, the phase transition point is  $V_i^{\text{th}} = 0.5$ , and the first two bands for  $V_i$  below and above the threshold value  $V_i^{\text{th}}$  are shown in Fig. 1. With the increase

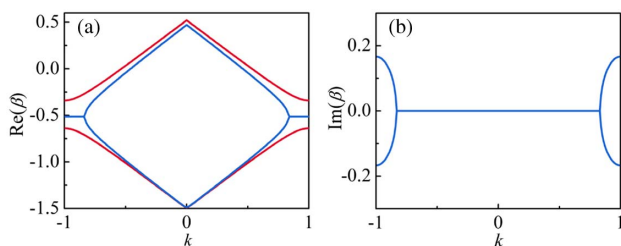


**Fig. 1.** (a) Photonic band structure for FSE with PT-symmetric periodic potential, when  $V_i = 0.4$  (red line) and  $0.55$  (blue line). (b) Imaginary parts of the band structure for  $V_i = 0.55$ .

of  $V_i$ , the band gap becomes narrower and disappears at the threshold value. When  $V_i > V_i^{\text{th}}$ , complex eigenvalues appear in the first two bands of the band structure. The dynamic process of the band structure with a periodic PT potential is quite similar to those in the ordinary Schrödinger equation reported previously [20,23,24]. However, there is a remarkable difference in that the first band is almost linear around  $k = 0$ , especially since all the bands become completely linear at the phase transition point [26]. The linear bands mean diffraction-free propagation of the beam due to the zero second-order derivative around  $k = 0$ .

Now we focus on the stationary soliton solutions to Eq. (1). They can be obtained from Eq. (1) in the form of  $\psi(z, x) = \phi(x) \exp(i\beta z)$ , in which  $\phi(x)$  is a complex function that describes the soliton shape, and  $\beta$  is the corresponding real propagation constant. The stationary soliton solutions were obtained through the squared operator method (SOM) described in Ref. [28]. This method consists of the iterative calculation of the solitary waves using the expression  $\phi^{(n+1)} = \phi^{(n)} - [\mathcal{M}^{-1} \mathcal{L}_1^{\dagger} \mathcal{M}^{-1} \mathcal{L}_0 \phi^{(n)}] dz$ , where  $\mathcal{L}_0 = -(-d^2/dx^2)^{\alpha/2} + V(x) + |\phi|^2 - \beta$ , and  $\mathcal{L}_0 \phi = 0$  for the exact soliton solutions.  $\mathcal{L}_1(\delta\phi) = \mathcal{L}_0(\phi + \delta\phi)$  is the result of linearizing  $\mathcal{L}_0$  by assuming a small perturbation  $\delta\phi \ll \phi$ . The acceleration operator  $\mathcal{M} = [c + (-d^2/dx^2)^{\alpha/2}]$  is introduced to speed up the convergence, in which  $c$  is a positive constant.

When the soliton solutions are obtained, the highest concern is their stability, that is, whether they are stable against small perturbations. Therefore, we perturb the soliton solutions as  $\psi(x, z) = e^{i\beta z}[\phi(x) + v(x)e^{\lambda z} + w^*(x)e^{\lambda^* z}]$ , where  $|v|, |w| \ll |\phi|$  are the perturbation functions, and  $\lambda$  indicates the perturbation growth rate. By substituting the perturbed solutions into Eq. (1) and linearizing, we obtain the linear eigenvalue problem

$$i \begin{pmatrix} \mathcal{L} & \phi^2 \\ -\phi^{*2} & -\mathcal{L}^* \end{pmatrix} \begin{pmatrix} v \\ w \end{pmatrix} = \lambda \begin{pmatrix} v \\ w \end{pmatrix}, \quad (3)$$

where  $\mathcal{L} = -(-d^2/dx^2)^{\alpha/2} + 2|\phi|^2 + V(x) - \beta$ . This eigenvalue problem can be solved by the Fourier collocation method or the Newton-conjugate-gradient method [29]. If eigenvalues  $\lambda$  with positive real parts exist, the solitons are linearly unstable; otherwise, they are stable.

We first consider solitary waves in the semi-infinite gap under unbroken PT symmetry for  $V_i < 0.5$ . We numerically construct the localized solutions by SOM. Figure 2(a) shows a typical field profile of such a soliton. Compared to the ordinary NSE in Ref. [24], the NFSE here has soliton solutions enduring stronger modulation induced by lattice potentials, which is caused by the weak diffraction of FSE that is discussed in the diffraction relation of the lattice above. Figure 2(b) displays the corresponding soliton profile of  $|\tilde{\phi}(k)|$  in the inverse space, which is obtained by the Fourier transform of  $\phi(x)$ . Apparently, the spectral distribution is not symmetric with respect to  $k = 0$ , and the peak values occur when the value of  $k$  is even. Such a phenomenon has been explained before through analyzing the coupling strength induced by the PT-symmetric potential in the inverse space [26]. The soliton solutions can exist with real propagation constants in spite of the existence of gain and loss, that is, because there are transverse power flows within

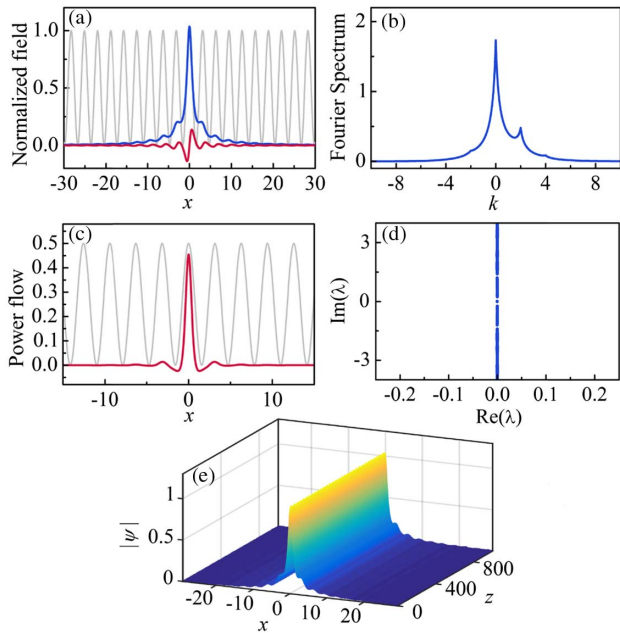


**Fig. 2.** (a) Soliton field profile (real part: blue line, imaginary part: red line) for  $\beta = 0.8$ . (b) The spectral distribution  $|\hat{\phi}(k)|$  in the inverse space. (c) Transverse power flow (red line) of the soliton. (d) Spectrum of the linearization operator for the soliton solution in (a). (e) Stable propagation perturbed with weak noise. The light gray line in (a) and (d) represents the scaled real part of the potential. For all cases,  $V_i = 0.4$  and  $A = 1$ .

them, which are quantified as the transverse power-flow density  $S = (i/2)(\phi\phi_x^* - \phi^*\phi_x)$ . Figure 2(c) displays the transverse power-flow density profile in the solitons. Obviously, the power flow is positive around the centers of waveguides, while it becomes negative in the regions between channels. This means that the direction of power flow is changed, and the energy always flows from gain to loss regions. On the other hand, the soliton stability is also examined by linear stability analysis on the basis of Eq. (3). Figure 2(d) shows the spectrum of the linearization operator for the soliton solution in Fig. 2(a). Perturbation growth rate  $\lambda$  has the largest real part  $\text{Re}\{\lambda\}_{\max} = 0$ , which means that the soliton solution in Fig. 2(a) is stable. In order to check the soliton stability, we conduct the propagation dynamics of solitons under weak perturbations. The stable solitons can repair and keep their shape under perturbations, as they do in complex systems [30]. A stable evolution is shown in Fig. 2(e) when  $V_i = 0.4$  and  $\beta = 0.8$ . In the initial condition, the stationary soliton solution is perturbed by white Gaussian noise, and the noise power is valued as 0.01.

It is worth noting that soliton solutions are also found when the PT symmetry is broken, which is shown in Fig. 3(a). This is because part of the band structure is still real, even above the phase transition point, which is illustrated in Fig. 1. The Floquet–Bloch decomposition of the solitons is primarily occupied by the eigenmodes with real eigenvalues that are located around  $k = 0$ . Moreover, in a nonlinear system, the nonlinearity can transform some eigenvalues of the band structure from complex to real [31]. This effect is conducive to the existence of solitons with real propagation constants in broken PT

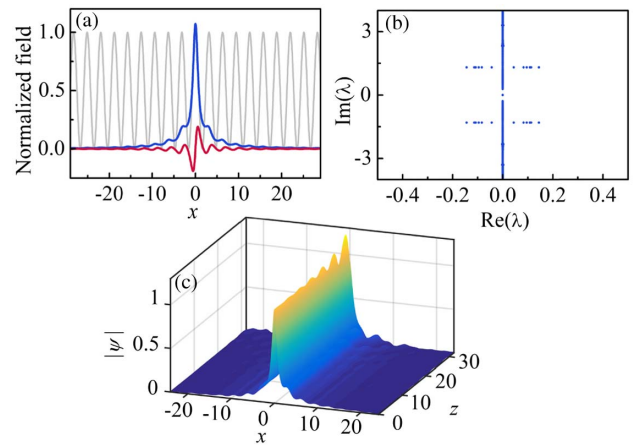


**Fig. 3.** (a) Soliton field profile (real part: blue line, imaginary part: red line). The light gray line denotes the real part of the potential. (b) The perturbation growth rate profile for the soliton solution in (a). (c) Unstable PT soliton propagation perturbed with weak noise. In all cases,  $V_i = 0.55$  and  $\beta = 0.8$ .

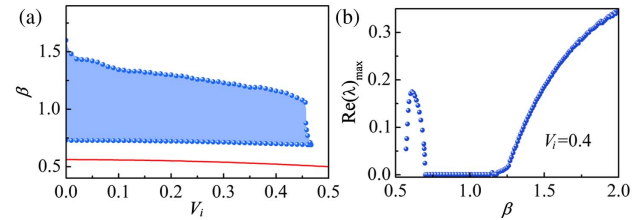


**Fig. 4.** (a) Domains of stability on the plane  $(\beta, V_i)$  for 1D solitons. Solitons are stable in the blue region. The red line denotes the lower edge of the semi-infinite forbidden gap. (b) The maximum real part of perturbation growth rate versus  $\beta$  for  $V_i = 0.4$  and  $A = 1$ .

symmetry. However, the linear stability analysis reveals that the solitons in such a system are not stable. For the soliton solution in Fig. 3(a), the corresponding values of perturbation growth rates are displayed in Fig. 3(b), and the maximal real part of  $\lambda$  is  $\text{Re}\{\lambda\}_{\max} = 0.14$ . The propagation dynamics of the perturbed soliton can also confirm this instability, as shown in Fig. 3(c). The perturbation is a white Gaussian noise with power of 0.01.

The entire existence domain of stable 1D solitons is performed in the  $(\beta, V_i)$  plane, as shown in Fig. 4(a). With the increase of  $V_i$ , the stability domain is at first gradually narrowed and then drastically shrinks when  $V_i > 0.45$ . It completely disappears when  $V_i > 0.467$ , which is slightly below the symmetry breaking point  $V_i^{\text{th}} = 0.5$ . The lower border of the stability domain is slightly decreased with the increase of  $V_i$ , and the variation of the stability domain is mainly determined by its upper border. From the results in Fig. 4(a), we can see that the stability domain of the solitons gets narrower with the increase of loss/gain strength in PT-symmetric lattices. A typical dependence of  $\text{Re}\{\lambda\}_{\max}$  on the propagation constant  $\beta$  is shown in Fig. 4(b) for  $V_i = 0.4$ . The typical normalized decay distance for unstable soliton solutions can be approximately valued as  $z \sim 1/\text{Re}\{\lambda\}_{\max}$ . The plot confirms that a linear stability analysis predicts stable 1D-soliton solutions



[i.e., with  $\text{Re}\{\lambda\}_{\max} = 0$ ] that can be examined by the direct propagation of the perturbed solutions.

### 3. TWO-DIMENSIONAL SOLITONS

Finally, we extend the analysis to the two-dimensional NFSE with PT symmetry. The 2D NFSE can be written as

$$i \frac{\partial \psi}{\partial z} - \left( -\frac{\partial^2}{\partial x^2} - \frac{\partial^2}{\partial y^2} \right)^{\alpha/2} \psi + V(x, y)\psi + |\psi|^2\psi = 0. \quad (4)$$

The PT-symmetric potential has the form  $V(x, y) = A\{\cos^2 x + \cos^2 y + iV_i[\sin(2x) + \sin(2y)]\}$ , which satisfies  $V(x, y) = V^*(-x, -y)$ . The 2D band structure is displayed in Fig. 5(a) for  $A = 4$  and  $V_i = 0.2$ . As in the one-dimensional case, the diffraction relation of the first band is almost linear around the band center, as shown in the inset of Fig. 5(a). The phase transition point is  $V_i^{\text{th}} = 0.5$ ; above this point the first two bands merge together, and complex eigenvalues occur in the surrounding region of the first Brillouin zone.

A 2D-soliton solution with a propagation constant in the semi-infinite gap is depicted in Fig. 5(b). We can see that the soliton intensity is mainly distributed in multiple cells. This distribution is more extensive relative to the single-cell distribution of solitons in the ordinary NSE [24,32]. The linear stability suggests that the soliton in Fig. 5(b) is stable for  $\text{Re}\{\lambda\}_{\max} = 0$ . Figure 5(c) shows the profile of the soliton in the inverse space. The spectrum is asymmetric with respect to  $k_x = 0$  or  $k_y = 0$ , and sharp peaks are exhibited at special locations where both  $k_x$  and  $k_y$  are even for the  $\pi$  period of the lattice. The reason for this feature is similar to that of the one-dimensional case. For the existence of gain and loss, the transverse power flow is required to maintain the energy balance within the soliton. The power flow is quantified by the Poynting vector  $\mathbf{S} = (i/2)(\phi \nabla \phi^* - \phi^* \nabla \phi)$ , which is vividly

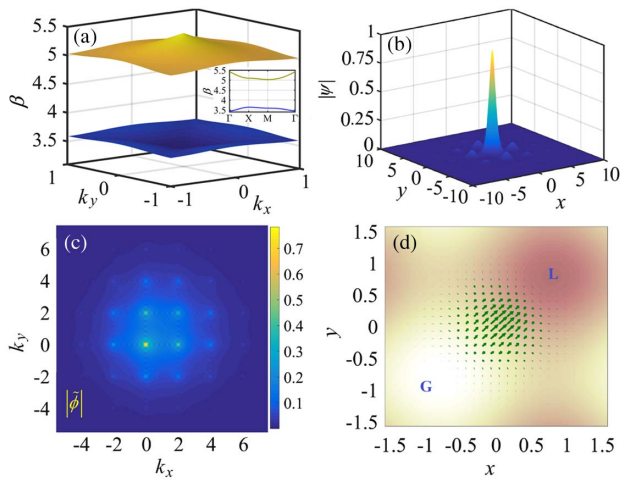


**Fig. 5.** (a) Band structure of a 2D-PT potential for Eq. (4) in linear form. The inset displays the band structure in the reduced Brillouin zone. (b) The profile of a 2D soliton when  $\beta = 5.55$ . (c) The spectral profile  $|\hat{\phi}(k_x, k_y)|$  in the inverse space. (d) Transverse power flow (indicated by arrows) for the soliton in (b) within one cell. “L” and “G” indicate the loss and gain regions, respectively. For all cases,  $A = 4$  and  $V_i = 0.2$ .

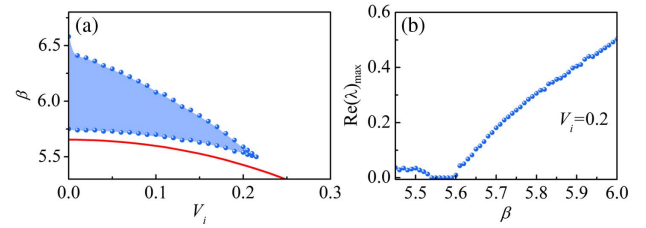


**Fig. 6.** (a) Domains of stability on the plane  $(\beta, V_i)$  for 2D solitons. Solitons are stable in the blue region. The red line denotes the lower edge of the semi-infinite forbidden gap. (b) Real part of perturbation growth rate versus  $\beta$  for  $A = 4$  and  $V_i = 0.2$ .

depicted in Fig. 5(d). Obviously, the energy inside the soliton flows from the gain region to the loss region.

The stability property of 2D-soliton solutions is also investigated by exploring their stability domains. As in the 1D case, the linear stability analysis of 2D solitons is performed, and the 2D form of Eq. (3) can be obtained. For the 2D version of Eq. (3), limited by the computer memory, the standard matrix eigenvalue solvers are only appropriate for a small number of transverse points. As a result, such a procedure cannot guarantee sufficient accuracy. Instead, here we use the iteration method put forward in Ref. [33] and obtain the eigenvalues with maximum real parts and the corresponding eigenfunctions of  $\mathcal{L}$ . Figure 6(a) displays the existence domain of a stable 2D soliton in the  $(\beta, V_i)$  plane. The stability domain shrinks quickly with the increase of  $V_i$  and completely disappears when  $V_i > 0.215$ . Both the upper and lower cutoffs decrease with the increase of  $V_i$ . The lower cutoff of the stability domain and the lower edge of the semi-infinite forbidden gap of the lattice have almost the same variation tendency with the variable  $V_i$ . Specifically, the dependence of  $\text{Re}\{\lambda\}_{\max}$  on the propagation constant  $\beta$  is characterized in Fig. 6(b) for  $V_i = 0.2$ . The stability domain is  $\beta \in [5.54, 5.59]$ , where the perturbation growth rate satisfies  $\text{Re}\{\lambda\}_{\max} = 0$ . All results obtained by the linear stability analysis can be confirmed by direct evolution of the perturbed soliton solutions.

### 4. CONCLUSION

We have studied one- and two-dimensional solitons in a new system of the NFSE in PT-symmetric lattices for a Lévy index of  $\alpha = 1$ . In real space, the solitons endure strong modulations induced by the lattice potential for the weak diffraction of the FSE. In the inverse space, the spectra experience sharp peaks at even-value wavenumbers due to the  $\pi$  period of the lattice. As the model becomes non-Hamiltonian, strong internal power flows emerge to substantially modify the soliton shapes, and the power flows always stream from gain regions to loss regions. When the PT symmetry is broken, soliton solutions still exist in spite of the fact that they are unstable. We show that the soliton parameters and the corresponding stability domains are dominated by the strength of the gains/losses of the PT-symmetric lattice. Therefore, the PT-symmetric lattices can act as effective tools to control the shapes, domains of existence, and stability domains of solitary waves in NFSE systems.

**Funding.** National Natural Science Foundation of China (NSFC) (61525505, 11774310); Natural Science Foundation of Shaanxi Province (2015KCT-06).

## REFERENCES

- N. Laskin, "Fractional quantum mechanics," *Phys. Rev. E* **62**, 3135–3145 (2000).
- R. Herrmann, *Fractional Calculus: An Introduction for Physicists* (World Scientific, 2011).
- N. Laskin, "Fractional quantum mechanics and Lévy path integrals," *Phys. Lett. A* **268**, 298–305 (2000).
- N. Laskin, "Fractional Schrödinger equation," *Phys. Rev. E* **66**, 056108 (2002).
- B. A. Stickler, "Potential condensed-matter realization of space-fractional quantum mechanics: the one-dimensional Lévy crystal," *Phys. Rev. E* **88**, 012120 (2013).
- S. Longhi, "Fractional Schrödinger equation in optics," *Opt. Lett.* **40**, 1117–1120 (2015).
- Y. Zhang, X. Liu, M. R. Belić, W. Zhong, Y. Zhang, and M. Xiao, "Propagation dynamics of a light beam in a fractional Schrödinger equation," *Phys. Rev. Lett.* **115**, 180403 (2015).
- L. Zhang, C. Li, H. Zhong, C. Xu, D. Lei, Y. Li, and D. Fan, "Propagation dynamics of super-Gaussian beams in fractional Schrödinger equation: from linear to nonlinear regimes," *Opt. Express* **24**, 14406–14418 (2016).
- C. Huang and L. Dong, "Beam propagation management in a fractional Schrödinger equation," *Sci. Rep.* **7**, 5442 (2017).
- X. Huang, X. Shi, Z. Deng, Y. Bai, and X. Fu, "Potential barrier-induced dynamics of finite energy Airy beams in fractional Schrödinger equation," *Opt. Express* **25**, 32560–32569 (2017).
- Y. Zhang, H. Zhong, M. R. Belić, N. Ahmed, Y. Zhang, and M. Xiao, "Diffraction-free beams in fractional Schrödinger equation," *Sci. Rep.* **6**, 23645 (2016).
- B. Guo and D. Huang, "Existence and stability of standing waves for nonlinear fractional Schrödinger equations," *J. Math. Phys.* **53**, 083702 (2012).
- Q. Li and X. Wu, "Soliton solutions for fractional Schrödinger equations," *Appl. Math. Lett.* **53**, 119–124 (2016).
- Y. Wan and Z. Wang, "Bound state for fractional Schrödinger equation with saturable nonlinearity," *Appl. Math. Comput.* **273**, 735–740 (2016).
- C. Huang and L. Dong, "Gap solitons in the nonlinear fractional Schrödinger equation with an optical lattice," *Opt. Lett.* **41**, 5636–5639 (2016).
- J. Xiao, Z. Tian, C. Huang, and L. Dong, "Surface gap solitons in a nonlinear fractional Schrödinger equation," *Opt. Express* **26**, 2650–2658 (2018).
- C. M. Bender and S. Boettcher, "Real spectra in non-Hermitian Hamiltonians having PT symmetry," *Phys. Rev. Lett.* **80**, 5243–5246 (1998).
- C. E. Rüter, K. G. Makris, R. El-Ganainy, D. N. Christodoulides, M. Segev, and D. Kip, "Observation of parity-time symmetry in optics," *Nat. Phys.* **6**, 192–195 (2010).
- A. Guo, G. J. Salamo, D. Duchesne, R. Morandotti, G. Siviloglou, and D. Christodoulides, "Observation of PT-symmetry breaking in complex optical potentials," *Phys. Rev. Lett.* **103**, 093902 (2009).
- K. G. Makris, R. El-Ganainy, D. N. Christodoulides, and Z. H. Musslimani, "Beam dynamics in PT-symmetric optical lattices," *Phys. Rev. Lett.* **100**, 103904 (2008).
- S. V. Suchkov, A. A. Sukhorukov, J. Huang, S. V. Dmitriev, C. Lee, and Y. S. Kivshar, "Nonlinear switching and solitons in PT-symmetric photonic systems," *Laser Photon. Rev.* **10**, 177–213 (2016).
- X. K. Yao and X. M. Liu, "Beam dynamics in disordered PT-symmetric optical lattices based on eigenstate analyses," *Phys. Rev. A* **95**, 033804 (2017).
- K. G. Makris, R. El-Ganainy, D. N. Christodoulides, and Z. H. Musslimani, "PT-symmetric optical lattices," *Phys. Rev. A* **81**, 063807 (2010).
- Z. H. Musslimani, K. G. Makris, R. El-Ganainy, and D. N. Christodoulides, "Optical solitons in PT periodic potentials," *Phys. Rev. Lett.* **100**, 030402 (2008).
- Y. V. Kartashov, C. Hang, G. Huang, and L. Torner, "Three-dimensional topological solitons in PT-symmetric optical lattices," *Optica* **3**, 1048–1055 (2016).
- Y. Zhang, H. Zhong, M. R. Belić, Y. Zhu, W. Zhong, Y. Zhang, D. N. Christodoulides, and M. Xiao, "PT symmetry in a fractional Schrödinger equation," *Laser Photon. Rev.* **10**, 526–531 (2016).
- L. Dong and C. Huang, "Double-hump solitons in fractional dimensions with a PT-symmetric potential," *Opt. Express* **26**, 10509–10518 (2018).
- J. Yang and T. I. Lakoba, "Universally-convergent squared-operator iteration methods for solitary waves in general nonlinear wave equations," *Stud. Appl. Math.* **118**, 153–197 (2007).
- J. Yang, *Nonlinear Waves in Integrable and Nonintegrable Systems* (SIAM, 2010).
- X. M. Liu, X. K. Yao, and Y. D. Cui, "Real-time dynamics of the build-up of solitons in mode-locked lasers," *Phys. Rev. Lett.* **121**, 023905 (2018).
- Y. Lumer, Y. Plotnik, M. C. Rechtsman, and M. Segev, "Nonlinearly induced PT transition in photonic systems," *Phys. Rev. Lett.* **111**, 263901 (2013).
- S. Nixon, L. Ge, and J. Yang, "Stability analysis for solitons in PT-symmetric optical lattices," *Phys. Rev. A* **85**, 023822 (2012).
- J. Yang, "Iteration methods for stability spectra of solitary waves," *J. Comput. Phys.* **227**, 6862–6876 (2008).